ANALYSIS OF INTEGRATING SPHERE PERFORMANCE FOR IR ENHANCED DT LAYERING

by
R.B. STEPHENS and G. COLLINS

SEPTEMBER 1996

GA–A22477

ANALYSIS OF INTEGRATING SPHERE PERFORMANCE FOR IR ENHANCED DT LAYERING

by
R.B. STEPHENS and G. COLLINS[†]

[†]Lawrence Livermore National Laboratory

GA PROJECT 3748
SEPTEMBER 1996

ANALYSIS OF INTEGRATING SPHERE PERFORMANCE FOR IR ENHANCED DT LAYERING

Richard B. Stephens
General Atomics
PO Box 85608
San Diego, California, 92186-5608
(619) 455-3863, e-mail: rich.stephens@gat.com

G. Collins
Lawrence Livermore National Laboratory
P.O. Box 5508 (L-482)
Livermore, California 94550
(510) 423-2204

ABSTRACT

Absorbed IR energy can supplement the beta decay energy from DT ice to improve the driving force toward uniform layers. A significant problem with this approach has been to deliver the added IR energy with sufficient uniformity to enhance rather than destroy the uniformity of the ice layers. Computer modeling has indicated that one can achieve ~1% uniformity in the angular variation of the absorbed power using an integrating sphere containing holes large enough to allow external inspection of the ice layer uniformity. The power required depends on the integrating sphere size; a 25 mm diameter sphere requires ~35 mW of IR to deposit as much energy in the ice as the 50 mW/cm^3(35 μW total) received from tritium decay in DT. Power absorbed in the plastic can cause unacceptable ice-layer non-uniformities for the integrating sphere design considered here.

I. INTRODUCTION

Tritium decay energy in DT ice layers automatically produces uniformly thick layers inside cryotargets.[1] Concerns about the ultimate smoothness of such layers, as well as a desire to layer DD ice has led to investigation of alternate layering mechanisms which involve either supplementing the DT decay heat[2,3] or nullifying the effects of gravity.[4–6] IR heating has been demonstrated to layer ice in proof-of-principle experiments with cylindrical geometry.[7] In all the techniques which add heat, uniformity of heat distribution is critical. For IR heating, refraction and reflection of the incident radiation redistributes the incoming light in ways which are difficult to compensate (Fig. 1). The approach considered here is to put the cryotarget inside an integrating sphere (a highly reflecting, but non-specular cavity) so that every point on

the surface receives the same intensity and distribution of incident light. By symmetry then, the IR heating would be spherically (but not necessarily radially) uniform. We cannot use a perfect integrating sphere; inspection holes and localized light sources are necessary, and perturb the symmetry of the illumination.
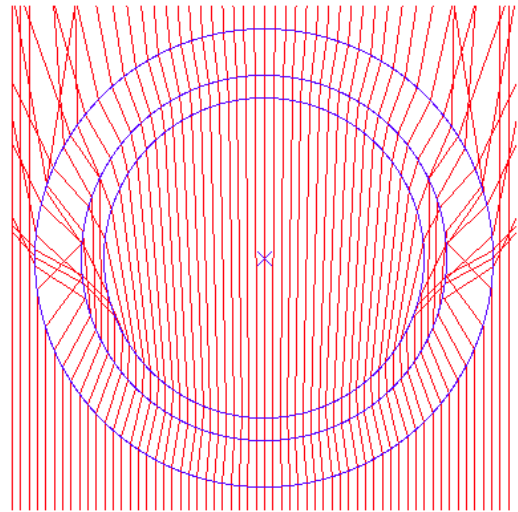

Fig. 1. Cross-section of a 2 mm o.d. cryotarget with 200 μm CH walls and 100 μm of condensed ice, with typical ray paths. Refraction concentrates light in some areas and depletes it from others. Reflection effects make this redistribution worse.

We have set up a computer simulation to investigate the magnitude of these fluctuations. Section II describes details of the experiment we are simulating. The calculation is broken into two parts: In Section III the brightness distribution of the interior of the integrating

sphere, and in Section IV the heating in each layer caused by a ray as a function of the angle between its source and the local surface normal. These two angular sensitivities are convolved together to produce a map of the heating distribution in the ice and plastic layers, described in Section V. The fluctuations and other parameters satisfy experimental constraints, as described in Section VI.

II. SIMULATION PARAMETERS

The dimensions of the cryotarget [Fig. 2(a)] were selected to be typical of those required for the National Ignition Facility (NIF): o.d. = 2 mm, CH wall thickness = 200 µm, and DT ice thickness = 100 µm. The indices of refraction of the two layers were taken to be 1.6 and 1.12 (for wavelengths around 3 µm), and the absorption to be 0.16 and 0.04 per layer thickness, respectively.

The dimensions of the integrating sphere [Fig. 2(b)] were determined by experimental constraints. It has an inside diameter = 25 mm. The three pairs of orthogonal inspection holes are the same size as the shell, 2 mm diameter. Only two pairs of holes are needed for inspecting the wall uniformity; the third was put in to give the best symmetry possible, and to allow for the insertion of a support structure (no support was included in the model). In a similar attempt to maximize symmetry, the light was injected at four tetrahedrally arranged points. The reflectance of the integrating sphere is ~96%, typical of Infragold™, LabSphere's infrared diffuse reflector. Light loss by absorption in the coating and by escape through the inspection holes is about equal, and limit the average photon to ~10 bounces before being lost.

The cryotarget intersects <1% of the photons leaving from any surface, so it has no influence on the brightness of the shell, and this calculation can be separated into two much easier segments. The brightness of the sphere, ignoring the cryotarget, is done in Section III, and the heating of the cryotarget as a function of the incident angle of light in Section IV. These are combined in Section V to give the heat distribution in each of the cryotarget layers.

III. INTEGRATING SPHERE BRIGHTNESS UNIFORMITY

The brightness distribution in the integrating sphere is determined from the Radiosity equation:

$$B(\Theta,\Phi) = R(\Theta,\Phi) \times \int \left(B(\theta,\phi) + I(\theta,\phi) \right) \times V(\theta,\phi,\Theta,\Phi) dA(\theta,\phi) \qquad (1)$$

where $B(\Theta,\Phi)$, $R(\Theta,\Phi)$, $I(\Theta,\Phi)$ are the brightness, reflectance, and light input, respectively, at point (Θ,Φ), and $V(\theta,\phi,\Theta,\Phi)$ is the visibility of point (θ,ϕ) from (Θ,Φ). This is solved by iterating the equation starting with $B(\Theta,\Phi) = 0$, and $I(\Theta,\Phi) = 1$ at the location of the light sources and 0 otherwise. Each iteration corresponds to one absorption/reemission step for a photon; at step i, the integral is the sum of light which arrived directly from the sources plus all possible paths with up to i bounces. Because the average photon bounces only 10 times, this calculation converges quickly; For the results shown in Fig. 3, we iterated Eq. (1) 30 times.

You can see in the figure that although the integrating sphere is very good at producing a uniformly bright surface, the shell is a little less bright around each of the
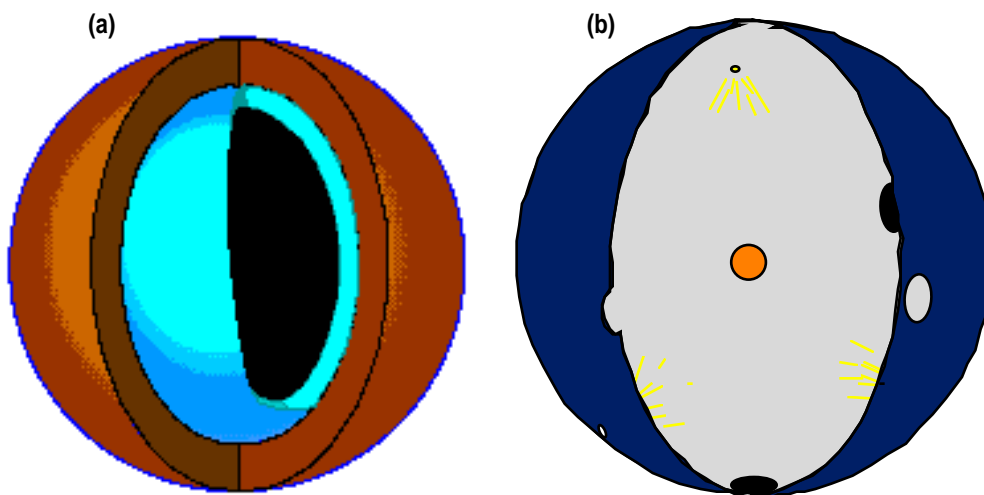

Fig. 2. (a) 2 mm o.d. Cryotarget with 200 µm thick CH walls and 100 µm thick DT ice. (b) 25 mm i.d. integrating sphere with three orthogonal pairs of 2 mm dia inspection holes, and four tetrahedrally arranged point light sources.
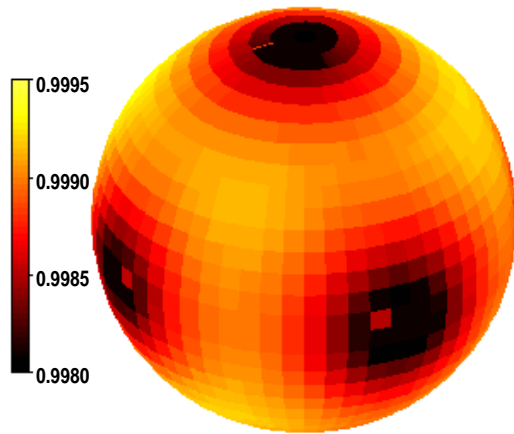
Fig. 3. Calculated brightness map of interior of integrating sphere. The inspection holes are black, but otherwise the brightness varies <0.1%.

inspection holes. That is a tiny effect. In addition, the area opposite each of the light sources is slightly brighter than the equivalent point near the light source; that effect is too small to show in this figure. This data is used in Section V to calculate the heating distribution of the cryotarget layers.

IV. ANGULAR DEPENDENCE OF CRYOTARGET HEATING

The heating caused by each ray depends on the path it takes. An Excel spreadsheet model was put together to calculate the heating at the center of each layer as a function of the polar angle of source of the ray, $h(\zeta)$. Although the angular dependence of the heating, $h(\zeta)$ is the same for every point, because of the spherical symmetry of the shell, the relationship between the local surface normal, ζ, and the (Θ,Φ) coordinate system by which the illumination is defined is different for every point on the shell. The actual heat received by each point is determined in Section V by convolving $h(\zeta)$ with $B(\zeta(\Theta,\Phi))$.

The heating calculation was done for each polarization separately, and the result summed. The absorption in each layer was calculated including multiple reflections within each layer, and reflections back from adjacent layers. We took the power from each ray to be deposited in the layer at the midpoint of its travel. Because the rays lose energy to adjacent layers with every reflection, as well as by absorption within the layer, we took that path length as the power absorbed divided by the absorption strength. That path length was used to determine the point at which the ray had entered the layer, and then to backtrack to estimate the location of its source.

Because of multiple reflections, the sources were not nearly so localized as this procedure assumes, so the structures shown in the figures below should be considerably smeared out. That would have the consequence of reducing the heating fluctuations shown in the next section.

Figure 4(a) shows that total internal reflection prevents some of the rays from reaching the ice layer. In addition, absorption in the plastic layer and reflection at the plastic ice layer reduce the amount of light reaching the ice layer. As a result, ~40% of the incident light is absorbed in the plastic, and only 1.8% in the ice.

The results of the spreadsheet calculations, $h(\zeta)$, for the ice and the plastic layers are shown in Fig. 5. Heating is dominated by rays from sources near or below the local horizon. These are the rays which have the longest path lengths in the shell. Rays coming from 90° or more never get into the ice layer, so that distribution is cut off at shorter angles.

V. HEATING UNIFORMITY OF CRYOTARGET LAYERS

The heating of the shell, $H(\Theta,\Phi)$, is determined from Eq. (2), and the results plotted in Fig. 6(a) for the plastic layer and 6(b) for the ice layer.

$$H(\Theta,\Phi) = \int h(\zeta(\Theta,\Phi,\theta,\phi))\, B(\theta,\phi)\, dA(\theta,\phi) \qquad (2)$$

The symmetry of the fluctuations should have the same cubic symmetry as that of the integrating sphere, with cooler regions away from the inspection holes. The pattern is roughly as expected, with fluctuations in temperature ~±1%. In addition, there are polar bands, which seem too strong to be real. They may just be an artifact of the finite element calculations, but they did not show up in the sphere brightness case.

Fluctuations in local heating of the plastic of ~ 1% cause fluctuations in the temperature difference across the shell. Assuming sufficient light to equal D-T beta decay heating (50 mW/cm^3), 0.5 mW/cm^2 is absorbed in the ice, and 10 mW/cm^2 in the plastic. This causes temperature gradients of 0.001 K and 0.2 K respectively. A 1% variation in the heat absorbed in the plastic causes a 0.002 K variation in the temperature of its inside surface. However, this is larger than the total temperature gradient across a uniform ice layer. For the simple integrating sphere and the thick walled shell modeled here, we would expect the hottest locations of the shell to be ice free.

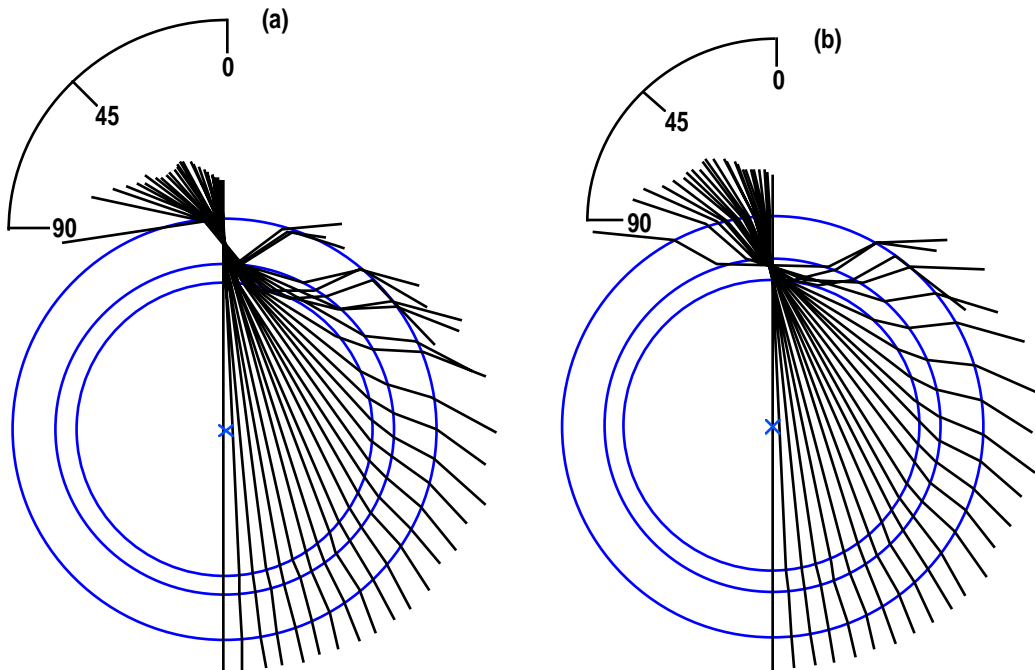This calculation suggests that illumination non-

Fig. 4. Paths of all rays going through a point in (a) the plastic layer, and (b) the ice layer. Multiple reflections are not shown, but were included in the calculation. Notice that total internal reflection prevents some rays from ever reaching the ice layer.
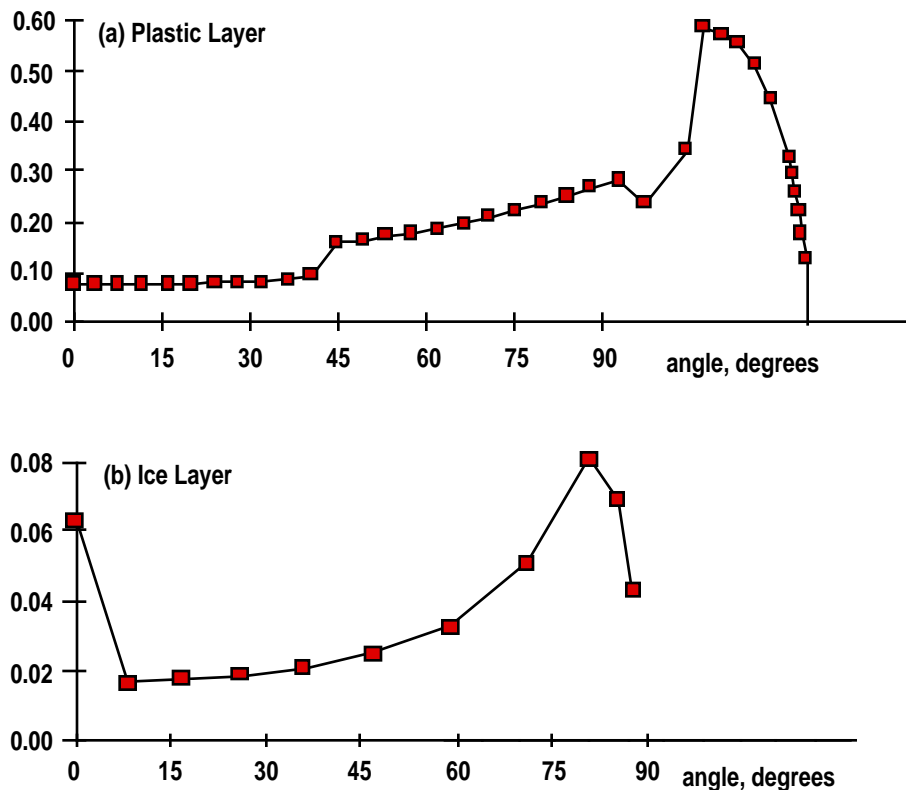

Fig. 5. Power absorbed in (a) the plastic layer, and (b) the ice layer as a function of the angle between the source and the local surface normal.
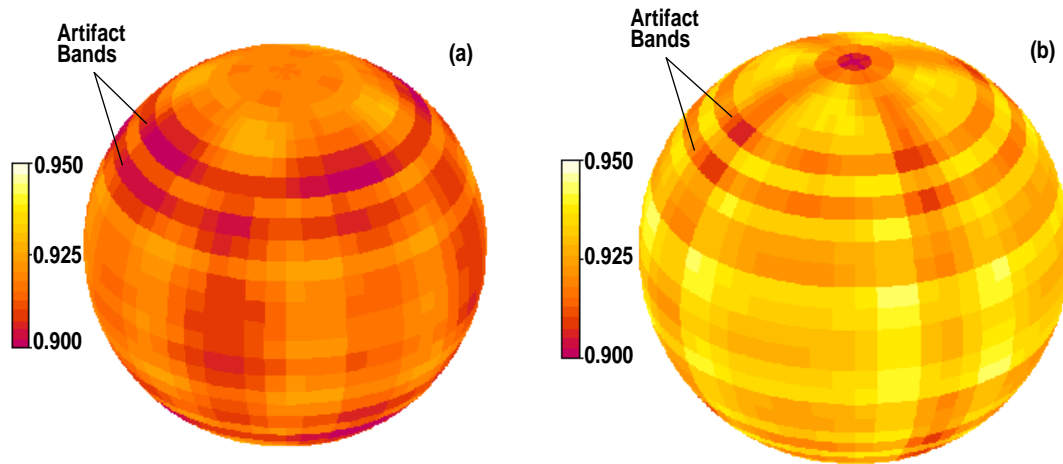
Fig. 6. Normalized heat input into (a) plastic layer and (b) plastic layer as a function of location on the cryotarget. The values vary by ~±1%. A pair of horizontal cool bands around each pole at ~60° latitude are artifacts of the calculation.

uniformities must be reduced to ~ 1/100%, or the plastic absorption strength reduced by ~100 times, to achieve few percent uniformity in the ice wall thickness. A more sophisticated integrating sphere, with highly reflecting hot windows would reduce the variation proportional to the reflectance of the windows, and a thinner shell wall would reduce the variation proportional by at least the square of the wall thickess. With modest care in the integrating sphere design, it should be feasible to satisfactorily layer shells with ~50 μm walls.

VI. EXPERIMENTAL FEASIBILITY

The integrating sphere is very wasteful of light. The shell intercepts <1% of the light emitted from the surface of the sphere, and absorbs <2% of that light in the ice layer. Since photons bounce ~10× before escaping, they get ten chances to be absorbed in the ice layer, and 0.1% of the light injected is absorbed in the ice. Beta decay heats DT ice at 50 mW/cm^3; that corresponds to 35 μW in this modeled cryotarget. A 35 mW laser is required to provide heating equal to beta heating of DT.

Since virtually all the power is lost in the integrating sphere surface or through the inspection holes, the power required scales with the square of those dimensions.

Since refraction and absorption in the plastic layer substantially reduce the heat getting to the ice layer, any reductions in plastic thickness, or absorption would increase the power deposited in the ice, but would require redoing the modeling with new assumptions to predict the size of the change.

Several potential problem areas were not examined in this work:

Since the shell is conducting ~9 mW/cm^2 into the surrounding gas, there will be a temperature gradient in the gas which modifies the uniformity of the outside temperature of the shell. Convection effects could cause systematic gradients in the outside shell temperature.

VII. SUMMARY

An integrating sphere can be used to heat the ice layer of a NIF capsule with uniformity, ±1%. Assumptions in constructing the computer simulation were conservative and would only increase the calculated perturbations.

The sphere diameter used in this study, 25 mm, can fit in the current experimental apparatus. An IR assisted layering experiment would require a >35 mW light source. Such an experiment is under construction.

Much more heat is deposited in the plastic layer of the cryotarget than in the ice layer. Any irregularities in that layer will affect the underlying ice temperature. In addition, that heat must be dissipated into the surrounding gas, and buoyancy effects there could also distort the ice temperature. Reducing the plastic thickness from the values used in this work could reduce those problems.

ACKNOWLEDGEMENTS

Dave Bernat, GA, produced the sphere mapping of the temperature distributions. This is a report of work

REFERENCES

1. J.K. Hoffer and L.R. Foreman, *Phys. Rev. Lett.* **60**, 1310 (1988); A.J. Martin, R.J. Simms, and R.B. Jacobs, *J. Vac. Sci. Technol. A* **6** 1885 (1988).

2. C.M. Chen, T. Norimatsu, Y. Tsuda, T. Yamanak, and S. Nakai, *J. Vac. Sci. Technol. A11* 33781 (1993).

3. G. Collins *et al ,* ICF Annual Report **3**, 81 (Lawrence Livermore National Laboratory, Livermore, California, UCRL-LR-105820-93 (1993).

4. S. Sacks and D. Darling, *Nucl. Fusion* **27** 447 (1987).

5. P. Parks and R. Fagaly, private communication.

6. K. Kim and D.L. Kratin, *J. Appl. Phys.* **61** 2729 (1988).

7. G.W. Collins, D.N. Bittner, E. Monsler, S. Letts, E.R. Mapoles, T.P. Bernat, *J. Vac. Sci. Technol. A14* 2897 (1996).